# Semianalytical Finite Element Analysis of Active Damping in Smart Cylindrical Shells

C. Saravanan, N. Ganesan and V. Ramamurti

*Journal of Vibration and Control* 2000 6: 849
DOI: 10.1177/107754630000600603

# Semianalytical Finite Element Analysis of Active Damping in Smart Cylindrical Shells

C. SARAVANAN
N. GANESAN
V. RAMAMURTI
*Machine Dynamics Laboratory, Department of Applied Mechanics, Indian Institute of Technology, Madras- 600 036, India*

(Received 7 December 1998; accepted 1 December 1999)

*Abstract:* Active damping in a smart cylindrical shell using piezoelectric sensors/actuators is studied. The electrodes on the sensors/actuators are spatially shaped to reduce spillover between circumferential modes. A three-noded, isoparametric, semianalytical finite element is developed and used to model the cylindrical shell. The element is based on a mixed piezoelectric shell theory that makes a single layer assumption for the displacements and a layerwise assumption for the electric potential. The effects of axial and circumferential mode number, length to radius ratio, radius to thickness ratio of the shell, percentage of the area of the shell covered with piezoelectric material, and the location of the collocated sensor/actuator on the shell on the active damping ratio of the shell are studied.

*Key Words:* Smart structures, active vibration control, finite element analysis, modal sensors

## NOMENCLATURE

| | | |
|---|---|---|
| $[\bar{C}]$ | = | elasticity matrix |
| $[C_a]$ | = | the active damping matrix |
| $\{D\}$ | = | electric displacement vector |
| $[e]$ | = | piezoelectric matrix |
| $\{E\}$ | = | electric field vector |
| $F_m$ | = | mechanical force |
| $F_Q$ | = | electric force |
| $G_F$ | = | feedback factor |
| $[K_{uu}]$ | = | structure stiffness matrix |
| $[K_{u\phi}], [K_{\phi\phi}]$ | = | piezoelectric matrices |
| $[M]$ | = | mass matrix |
| $N_i$ | = | shape function corresponding to the $i$th mode |
| $\{Q\}$ | = | applied charge density on the surface $A_p$ |
| $\{S\}^T$ | = | mechanical strains $= \{S_{ss}, S_{\theta\theta}, S_{\theta z}, S_{zs}, S_{s\theta}\}^T$ |
| $t_P$ | = | thickness of the piezoelectric layer |
| $t_s$ | = | piezoelectric sensor thickness |
| $u_o, v_o, w_o$ | = | the displacements at middle surface of the laminate |
| $\{\bar{u}\} = \{u \quad v \quad w\}^T$ | = | displacements |

*Journal of Vibration and Control*, 6: 849-873, 2000

$V_s$ = volume of base structural material
$V_{pi}$ = volume of actuator layer
$V_{po}$ = volume of sensor layer
$[\varepsilon]$ = electric permitivity matrix
$\lambda$ = the complex eigenvalue
$\{\sigma\}$ = mechanical stresses
$\psi_s, \psi_\theta$ = rotations of the laminate
$\rho$ = mass density
$\bar{\phi}$ = potential on the $\cos m\theta$-shaped electrode
$\zeta$ = active damping ratio
$\phi$ = electric potential

Subscripts

$m$ = $m$th circumferential mode
$j$ = $j$th layer
$i$ = $i$th node
$e$ = elemental

Superscripts

$s$ = sensor
$a$ = actuator

## 1. INTRODUCTION

In recent years, there has been an increasing interest in the development of smart structures for space and industrial applications. These structures become smart because they contain their own sensors, actuators, and control capabilities. Piezoelectric layers could be embedded in or bonded to the structural material to act as sensors or actuators. A significant amount of research has been conducted on the static/dynamic response of smart beams and plates. But research on the static/dynamic analysis of shells with piezoelectric layers is relatively scarce.

The finite element method (FEM) could be used in the analysis of smart structures as structures of arbitrary shapes that are very difficult to analyze using analytical methods could very easily be analyzed by FEM.

Allik and Hughes (1970) gave the finite element formulation for piezoelectric continua. They developed the tetrahedral piezoelectric finite element. Tzou and Tseng (1990) proposed a modified isoparametric hexahedral solid finite element with internal degrees of freedom to model thin piezoelectric continua. Tzou and Ye (1996) derived a laminated quadratic $C^o$ piezoelastic triangular doubly curved shell finite element using the layerwise constant shear angle theory. Heyliger, Pei, and Saravanos (1996) used a quadratic discrete layer shell element to model a cylindrical shell with piezoelectric layers. Saravanos (1997) proposed a mixed piezoelectric shell theory and derived an eight-noded doubly curved shell finite element based on it.

Static analysis of smart shells with piezoelectric layers has been reported by a few in the literature. Sonti and Jones (1996) modeled a piezoelectric actuator ring pasted on the surface of a cylindrical shell and studied the effect of piezoelectric actuator dimensions on

the magnitude of the static actuator force exerted. Xu and Noor (1996) modeled the coupled thermoelectroelastic response of multilayered hybrid composite cylindrical shell panels. They assumed a Fourier series expansion of the displacement, temperature, and electrode potential in the circumferential and axial directions. The response quantities were obtained using a modified Frobenius method and a sublayer method. Heyliger, Pei, and Saravanos (1996) used the FEM to obtain the static response of a cylindrical shell of revolution with a piezoelectric layer. They demonstrated the relationship between applied voltage (mechanical force) and induced displacement (voltage). Saravanos (1997) studied the effect of geometric parameters on the active and sensory response of a laminated cantilevered cylindrical shell panel with continuous piezoelectric layers/discrete piezoelectric patches.

Dynamic analysis (free vibration analysis and active vibration control) of smart shells with piezoelectric material is scantly reported in the literature. Tzou (1991) suggested a distributed modal identification and control theory for sensing and control of smart continua. Tzou and Howard (1994) proposed a generic piezothermoelastic theory for shell continua and discussed the applications of the theory to smart structures in sensing and control. No numerical studies were done in the two papers mentioned above. Callahan and Baruh (1996) suggested a method to study the contribution of individual modes to the piezoelectric output for a cylindrical shell of revolution. Hussein and Heyliger (1996) used a discrete layer theory that combines finite element approximations through the shell thickness with Fourier and/or power series in the axial and circumferential directions to model laminated cylindrical shells with piezoelectric layers. They reported the natural frequencies of the cylindrical shell for the axisymmetric mode only. Tzou, Bao, and Venkayya (1996) studied the effect of geometric parameters on the modal actuation factor, modal feedback factor, and controlled damping ratio for a cylindrical shell panel with arbitrarily located, quarterly segmented piezoelectric patch. They adopted analytical techniques to solve the governing equations. Tzou and Ye (1996) performed a free vibration analysis and also studied the distributed vibration control characteristics of a cantilevered smart semicircular cylindrical ring. They reported only a few numerical results. Sung, Chen, and Chen (1996) used the classical lamination theory (CLT) to model a cylindrical shell with piezoelectric layers. They used analytical methods to solve the governing equations. They suggested a method for design of modal sensors and actuators. These modal sensors (actuators) are capable of sensing (actuating) a particular axial mode corresponding to the first circumferential mode (beam mode) only. Feedback control was not implemented. Baruch and Abramovich (1997) developed a shell theory based on Kirchoff's assumptions, for anisotropic piezolaminated shells with spatially discrete sensors. They did the dynamic analysis for a cylindrical shell panel excited by a pair of actuators but presented very few numerical results.

From the above literature survey, it is seen that, to the authors' knowledge, active vibration control of shells of revolution has not been reported in the literature. Hence, it is attempted in this paper. Distributed modal sensors (Tzou, Zhong, and Natori, 1993) and actuators that have spatially shaped electrodes are used in this analysis. Use of these sensors and actuators reduces the problem of observation/control spillover between the circumferential modes. To improve the computational efficiency, a semianalytical finite element method is used for the analysis.

## 2. FORMULATION OF GOVERNING EQUATIONS

### 2.1. Kinematic Relations

A first-order shear deformation theory (FSDT) is considered for the displacements. A layerwise theory is considered for the electric potential.

$$\begin{aligned} u(s,\theta,z,t) &= u_o(s,\theta,t) + z\psi_s(s,\theta,z) \\ v(s,\theta,z,t) &= v_o(s,\theta,t) + z\psi_\theta(s,\theta,z) \\ w(s,\theta,z,t) &= w_o(s,\theta,t) \end{aligned} \tag{1}$$

$$\phi(s,\theta,z,t) = \sum_{j=1}^{\text{nlay}} \phi_j(s,\theta,t)\, \bar{\bar{N}}_j(z), \tag{2}$$

where $\bar{\bar{N}}_j(z)$ are considered to be linear interpolation functions, $u_o, v_o, w_o$ are the displacements at middle surface of the laminate. $\psi_s, \psi_\theta$ are the rotations of the laminate.

The variation in the $\theta$ direction is given by

$$\begin{Bmatrix} u_o \\ v_o \\ w_o \\ \psi_s \\ \psi_\theta \end{Bmatrix} = \sum_{m=0}^{\infty} \begin{bmatrix} \cos m\theta & & & & 0 \\ & \sin m\theta & & & \\ & & \cos m\theta & & \\ & & & \cos m\theta & \\ 0 & & & & \sin m\theta \end{bmatrix} \begin{Bmatrix} u_{om} \\ v_{om} \\ w_{om} \\ \psi_{sm} \\ \psi_{\theta m} \end{Bmatrix}$$

$$= [\bar{\theta}] \begin{Bmatrix} u_{om} \\ v_{om} \\ w_{om} \\ \psi_{sm} \\ \psi_{\theta m} \end{Bmatrix} \tag{3}$$

and

$$\phi_j = \sum_{m=0}^{\infty} \phi_{jm} \cos m\theta, \tag{4}$$

where subscript $m$ stands for the $m$th circumferential harmonic.

### 2.2. Constitutive Relations for a Piezoelectric Material

$$\{\sigma\} = [\bar{C}]\{S\} - [e]\{E\} \tag{5}$$

$$\{D\} = [e]^T \{S\} + [\varepsilon] \{E\}, \tag{6}$$

where

$\{\sigma\}$ = mechanical stresses

$\{S\}^T$ = mechanical strains = $\{S_{ss}, S_{\theta\theta}, S_{\theta z}, S_{zs}, S_{s\theta}\}^T$

$[\bar{C}]$ = elasticity matrix

$[e]$ = piezoelectric matrix

$[\varepsilon]$ = electric permitivity matrix

$\{D\}$ = electric displacement vector

$\{E\}$ = electric field vector

### 2.3. *Geometric Relationships*

The strain-displacement relations considered are for a doubly curved shell of revolution.

$$\{S\} = [\partial] \begin{Bmatrix} u \\ v \\ w \end{Bmatrix} \tag{7}$$

using equation (1) in equation (7),

$$\{S\} = [\bar{Z}] [\bar{\partial}] \begin{Bmatrix} u_o \\ v_o \\ w_o \\ \psi_s \\ \psi_\theta \end{Bmatrix}, \tag{8}$$

where $[\bar{Z}] = [[I] \quad z[I]]$ and $[I]$ is a $5 \times 5$ identity matrix.

The electric field-potential relations are given as

$$\{E\} = \begin{Bmatrix} E_s \\ E_\theta \\ E_z \end{Bmatrix} = \begin{Bmatrix} 0 \\ 0 \\ -\dfrac{\partial \phi}{\partial z} \end{Bmatrix} \approx \begin{Bmatrix} 0 \\ 0 \\ -\dfrac{\phi}{t_P} \end{Bmatrix}, \tag{9}$$

where $t_P$ = thickness of the piezoelectric layer. Since only the poling direction is considered, $E_s, E_\theta = 0$.

### *2.4. Finite Element Formulation*

A three-noded isoparametric semianalytical element is derived. The variation of the displacements and potential along the meridional direction is given by

$$\begin{Bmatrix} u_{om} \\ v_{om} \\ w_{om} \\ \psi_{sm} \\ \psi_{\theta m} \end{Bmatrix} = \sum_{i=1}^{3} \begin{bmatrix} N_i & & & & 0 \\ & N_i & & & \\ & & N_i & & \\ & & & N_i & \\ 0 & & & & N_i \end{bmatrix} \begin{Bmatrix} u_{omi} \\ v_{omi} \\ w_{omi} \\ \psi_{smi} \\ \psi_{\theta mi} \end{Bmatrix} = \sum_{i=1}^{3} [N] \{d_{mi}\} \tag{10}$$

and

$$\phi_{jm} = \sum_{i=1}^{3} N_i \phi_{jmi} , \tag{11}$$

where $N_i$ are the shape functions.

Rewriting equation (8),

$$\{S\} = [\bar{Z}] [\bar{\partial}] \sum_{m=0}^{\infty} \sum_{i=1}^{3} [\bar{\theta}] [N] \{d_{mi}\} \tag{12}$$

$$\{S\} = [\bar{Z}] \sum_{m=0}^{\infty} \left[\bar{\bar{\theta}}\right] \sum_{i=1}^{3} \left[\bar{\bar{\partial}}\right] [N] \{d_{mi}\} , \tag{13}$$

where $\left[\bar{\bar{\theta}}\right] = \begin{bmatrix} c & & & & & & & & 0 \\ & c & & & & & & & \\ & & s & & & & & & \\ & & & c & & & & & \\ & & & & s & & & & \\ & & & & & c & & & \\ & & & & & & c & & \\ & & & & & & & s & \\ & & & & & & & & c \\ 0 & & & & & & & & s \end{bmatrix}$ ; $c = \cos m\theta$, $s = \sin m\theta$.

Consider a multilayered structure with the outermost layers made of piezoelectric material. The total potential energy of the system is

$$P.E. = \frac{1}{2} \left[ \int_{v_s} \{S\}^T \{\sigma\} \, dv - \int_{v_{P_1}} \{E\}^T \{D\} \, dv + \int_{v_{P_1}} \{S\}^T \{\sigma\} \, dv \right.$$

$$- \int_{V_{Po}} \{E\}^T \{D\}\, dv + \int_{V_{Po}} \{S\}^T \{\sigma\}\, dv \Big] - \int_A \{\bar{u}\}^T \{F\}\, dA$$

$$- \int_{A_p} \{\phi\} \{Q\}\, dA, \tag{14}$$

where

$\{Q\}$ = applied charge density on the surface $A_p$.

$V_s$ = volume of base structural material

$V_{pi}$ = volume of actuator layer

$V_{po}$ = volume of sensor layer

$$\{\bar{u}\} = \{u \quad v \quad w\}^T$$

$$K.E. = \frac{1}{2} \rho \int_V \left\{\dot{\bar{u}}\right\}^T \left\{\dot{\bar{u}}\right\} dv, \tag{15}$$

where $\rho$ = density.

The governing equations are obtained using Hamilton's variational principle,

$$\delta \int_{t_1}^{t_2} (P.E. - K.E.)dt = 0. \tag{16}$$

Using equations (14) and (15) in the above equation, we get the governing equations in finite element form.

$$[M]_e \left\{\ddot{d}\right\}_e + [K_{uu}]_e \{d\}_e - \left[K^a_{u\phi}\right]_e \{\phi_a\}_e - \left[K^s_{u\phi}\right]_e \{\phi_s\}_e = \{F_m\}_e \tag{17a}$$

$$\left[K^a_{\phi u}\right]_e \{d\}_e + \left[K^a_{\phi\phi}\right]_e \{\phi_a\}_e = \{F_Q\}_e \tag{17b}$$

$$\left[K^s_{\phi u}\right]_e \{d\}_e + \left[K^s_{\phi\phi}\right]_e \{\phi_s\}_e = \{0\}. \tag{17c}$$

The subscript $a$ stands for actuator layer, and subscript $s$ stands for sensor layer. The definitions of the various matrices and the sign convention are similar to that in Allik and Hughes (1970).

For free vibration analysis, equations (17) could be assembled and written without differentiating between the sensor and actuator layers, in the form (Allik and Hughes, 1970),

$$[M] \left\{\ddot{d}\right\} + \left[K_{uu} - K_{u\phi} K^{-1}_{\phi\phi} K_{\phi u}\right] \{d\} = \{0\}. \tag{18}$$

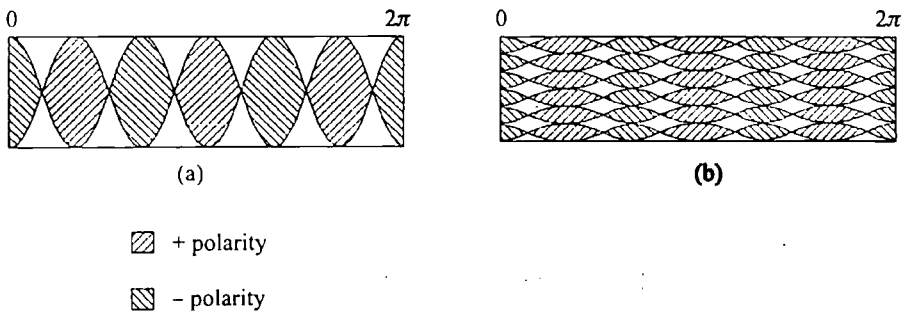


Figure 1. Shape of spatially distributed sensor/actuator electrode ($\cos 3\theta$ shape).

Note that the equations corresponding to the various circumferential harmonics are decoupled.

### *2.5. Active Control*

The inner piezoelectric layer is taken as the actuator and the outer piezoelectric layer as the sensor. The shape of the electrode surface is similar to that of Tzou, Zhong, and Natori (1993).

In the present study, each sensor/actuator pair is assumed to be collocated. Negative velocity feedback type of control is considered here.

Reconsidering the integral in equation (14), which resulted in the $[K_{u\phi}]_e$ matrices,

$$\int_{V_{Po}} \{\delta S\}[e]\{E\}\,dv = \sum_{m=0}^{\infty} \int_{V_{Po}} \{\delta d\}_e^T \left(\sum_{i=1}^{3} \left[\bar{\bar{\partial}}\right][N]\right)^T \left[\bar{\bar{\theta}}\right]^T [\bar{Z}]^T \times [e] \begin{Bmatrix} 0 \\ 0 \\ \dfrac{1}{t_p} \end{Bmatrix} \bar{\phi}\,dv, \tag{19}$$

where $t_p$ = thickness of the piezoelectric layer, $\bar{\phi} = \bar{\phi}(s, \theta)$ = constant = the potential on the $\cos m\theta$-shaped electrode.

Figure 1 shows six lobes as it represents the $\cos 3\theta$ shape. Similarly, a $2m$ lobe pattern would represent $\cos m\theta$ shape. The electrodes take the form of an array of $\cos m\theta$ shapes (Figure 1(b)) instead of a single $\cos m\theta$ shape (Figure 1(a)). In practice, the rate of change of strain in the axial direction for a particular mode is to be plotted. From this, the height of the cosine shapes in the electrodes are decided for that particular mode. Although this varies from mode to mode, the theoretical formulation remains unchanged and the above variation is an implementation issue. This is not addressed in the present paper. Lee and Moon (1990) showed that arbitrary electrode shapes could be obtained by using printed circuit board technology.

If the magnitude of strain is assumed to be invariant in the $s$ direction over each $\cos m\theta$ pattern of the electrode, then the above equation becomes

$$= \{\delta d\}_e^T \sum_{m=0}^{\infty} \left\langle \int_0^t \int_0^{2\pi} \int_0^1 \left( \sum_{i=1}^{3} \left[\bar{\bar{\partial}}\right][N] \right)^T \left[\bar{\bar{\theta}}\right]^T \left[\bar{Z}\right]^T [e] \right.$$

$$\left. \times \begin{Bmatrix} 0 \\ 0 \\ 1 \\ \overline{t_p} \end{Bmatrix} \cos m\theta \operatorname{sgn}(\cos m\theta)\, dv \right\rangle \bar{\phi}, \tag{20}$$

where $\operatorname{sgn}(\cos m\theta)$ is the signum function as defined in Tzou, Zhong, and Natori (1993). When the $\theta$ direction integration is performed, the expressions corresponding to the different circumferential harmonics get decoupled. When the above equation is used in the Hamilton's equation and the first variation is equated to zero, we get, for a particular circumferential harmonic, the term $\left\{\bar{\bar{K}}_{u\phi}\right\}_e \bar{\phi}$ instead of $[K_{u\phi}]_e \{\phi\}$. Here also it is to be noted that the expressions for the various circumferential harmonics get decoupled.

In the sensors, the converse piezoelectric effect is negligible and the external charge applied is zero, so the average potential over an electrode is given by (Tzou, 1991)

$$\bar{\phi}_s = \frac{t_s}{\varepsilon_{33} A_{\text{elec}}} \int_{A_{\text{elec}}} \lfloor e_{31} \quad e_{32} \rfloor \begin{Bmatrix} S_{ss} \\ S_{\theta\theta} \end{Bmatrix} dA, \tag{21}$$

where $A_{\text{elec}}$ is the area of the electrode. From Tzou, Zhong, and Natori (1993) for the shape of electrode considered, the above equation becomes

$$\bar{\phi}_s = \left\langle \frac{t_s}{\varepsilon_{33} A_{\text{elec}}} \sum_{m=0}^{\infty} \int_0^1 \int_0^{2\pi} \operatorname{sgn}(\cos m\theta) \cos m\theta \lfloor e_{31} \quad e_{32} \rfloor \left[\bar{Z}\right]_{z=z_0} \right.$$

$$\left. \times \left[\bar{\bar{\theta}}\right] \left( \sum_{i=1}^{3} \left[\bar{\bar{\partial}}\right][N] \right) dA \right\rangle \{d\}_e, \tag{22}$$

where $zo$ is the value of $z$ at the outer surface. In the above equation, the terms corresponding to the various circumferential harmonics get decoupled. Equation (22) could be written as

$$\bar{\phi}_s = \left\{\bar{\bar{K}}^s_{\phi u}\right\}^T \{d\}_e. \tag{23}$$

For negative velocity feedback control, we have

$$\bar{\phi}_a = -G_F \dot{\bar{\phi}}_s, \tag{24}$$

where $\dot{\bar{\phi}}_s$ is the time derivative of $\bar{\phi}_s$ and $G_F$ is the feedback factor.

Using equations (20), (14), (15) in equation (16), an equation analogous to equation (17a) is obtained.

$$[M]_e \left\{\ddot{d}\right\}_e + [K_{uu}]_e \{d\}_e - \left\{\bar{\bar{K}}^a_{u\phi}\right\}_e \bar{\phi}_a - \left\{\bar{\bar{K}}^s_{u\phi}\right\}_e \bar{\phi}_s = \{F\}_e \tag{25}$$

using equations (23) and (24) in equation (25),

$$[M]_e \left\{\ddot{d}\right\}_e + \left\{\bar{\bar{K}}^a_{u\phi}\right\}_e \left\{\bar{\bar{K}}^s_{\phi u}\right\}^T_e \left\{\dot{d}\right\}_e + \left([K_{uu}]_e - \left\{\bar{\bar{K}}^s_{u\phi}\right\}_e \left\{\bar{\bar{K}}^s_{\phi u}\right\}^T_e\right) \{d\}_e = \{F\}_e . \tag{26}$$

After assembling, equation (26) takes the form

$$[M]\left\{\ddot{d}\right\} + [C_a]\left\{\dot{d}\right\} + \left([K_{uu}] - \left\{\bar{\bar{K}}^s_{u\phi}\right\}\left\{\bar{\bar{K}}^s_{\phi u}\right\}^T\right)\{d\} = \{F\}, \tag{27}$$

where $[C_a]$ is the active damping matrix. If Rayleigh damping is also included, equation (27) takes the form

$$[M]\left\{\ddot{d}\right\} + [C]\left\{\dot{d}\right\} + [K^*]\{d\} = \{F\}, \tag{28}$$

where

$$[C] = [C_a + C_{\text{Rayleigh}}], \quad [K^*] = \left([K_{uu}] - \left\{\bar{\bar{K}}^s_{u\phi}\right\}\left\{\bar{\bar{K}}^s_{\phi u}\right\}^T\right).$$

To estimate the damping capability of the system, the damping ratio could be found out. There are three ways of finding out the damping ratio: (i) in time domain using the logarithmic decrement method, (ii) in frequency domain using the half power method, (iii) in frequency domain by the eigenvalue method. In this paper, the eigenvalue method is adopted. One major advantage of this method is that one can also comment on the stability of the system if the eigenvalues of the system are known. Writing equation (28) in state space after making $\{F\} = 0$, would result in the unsymmetric eigenvalue problem (Zheng, Ren, and Wang, 1997)

$$\begin{bmatrix} -C & -M \\ M & 0 \end{bmatrix} \begin{Bmatrix} d \\ \lambda d \end{Bmatrix} = \lambda \begin{bmatrix} K^* & 0 \\ 0 & M \end{bmatrix} \begin{Bmatrix} d \\ \lambda d \end{Bmatrix}, \tag{29}$$

where $\lambda$ is the complex eigenvalue.

Let $\lambda = \lambda_R + i\lambda_I$. Then the natural frequency $= \lambda_I$ rad/sec, and the damping ratio

$$\varsigma = \frac{-\lambda_R}{\sqrt{\lambda_R^2 + \lambda_I^2}}.$$

Table 1. Lowest 10 natural frequencies for free-free and closed-circuit boundary condition.

| | Natural Frequencies (Hz) | |
|---|---|---|
| | Heyliger, Pei, and Saravanos (1996) | Present Study |
| 1 | 31.26 | 30.32 |
| 2 | 53.72 | 53.83 |
| 3 | 88.64 | 85.77 |
| 4 | 134.50 | 133.7 |
| 5 | 170.42 | 164.4 |
| 6 | 229.61 | 226.4 |
| 7 | 276.52 | 265.8 |
| 8 | 343.27 | 335.8 |
| 9 | 407.28 | 389.8 |
| 10 | 478.64 | 464.7 |

It should be noted that for a particular cylindrical shell a $\cos m\theta$-shaped electrode would control only the $m$th circumferential harmonic. If more than one circumferential harmonic needs to be controlled, then sensors/actuators with the electrodes appropriately shaped to control each of those harmonics need to be stacked one above the other (though they should be electrically isolated from each other).

The height of each cosine pattern is modal and geometry dependent. But this does not change the theoretical derivation in any way, as only the magnitude and not the shape of the cosine function is changed.

In the case of cylindrical shells, the lowest natural frequencies are generally confined to a few circumferential harmonics. So the number of circumferential harmonics that one would be interested in controlling would be few.

## 3. VALIDATION

A two-layered cylindrical shell (titanium padded with a layer of PZT-4 on the outside), of dimensions length = $3.058 \times 10^2$ mm, inner radius = $2.89 \times 10^2$ mm, titanium layer thickness = 3 mm, and PZT-4 layer = 1 mm, is considered. The natural frequencies are found for the free-free mechanical boundary condition, and the closed-circuit electric boundary condition is considered. This is compared with those tabulated in Heyliger, Pei, and Saravanos (1996). Table 1 shows the lowest 10 natural frequencies of the above-mentioned shell.

## 4. NUMERICAL ANALYSIS

For the numerical study, a titanium cylindrical shell is considered. The sensor and actuator layers are assumed to be made of PZT-4. The material properties are obtained from Heyliger, Pei, and Saravanos (1996). The thickness of the titanium shell is kept at a constant value of 3 mm. The thickness of the piezoelectric layers are kept at a constant value of 20 $\mu$ m. For the numerical study, the following shell sizes are considered. Let $L^* = 3.048 \times 10^2$ mm and $R^* = 2.92 \times 10^2$ mm. Then the length and mean radius of the various shells are

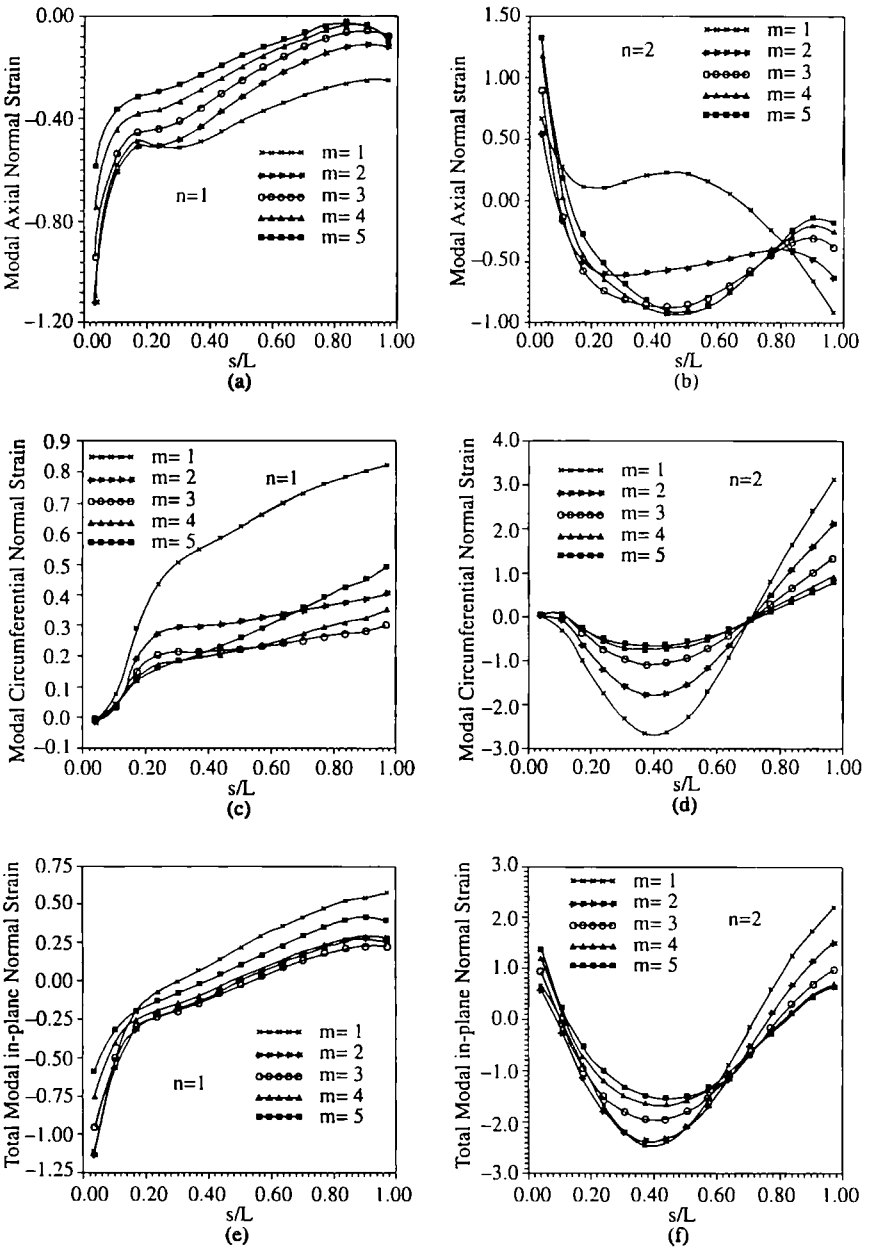


Figure 2. Variation of modal in-plane normal strain along the length of the shell for various circumferential and axial mode numbers.

Shell I: Length = $L^*$, Inner Radius=R*(short shell)

Shell II: Length = $1.3L^*$, Inner Radius = $1.3R^*$

Shell III: Length = $1.7L^*$, Inner Radius = $1.7R^*$

Shell IV: Length = $2L^*$, Inner Radius = $2R^*$

Shell V: Length = $1.3L^*$, Inner Radius = $R^*$

Shell VI: Length = $1.7L^*$, Inner Radius = $R^*$

Shell VII: Length = $2L^*$, Inner Radius = $R^*$ (Tall shell)

The clamped-free boundary condition is considered for the numerical study. Unless specified, the entire shell is assumed to be covered with piezoelectric sensors/actuators.

## 5. RESULTS AND DISCUSSION

In any practical structure with vibration control, the damping due to the negative velocity feedback is superimposed over the structural damping inherent in the structure. The structural damping could be modeled as Rayleigh damping for structures with low structural damping. Since the structure considered in this paper is assumed to behave linearly, the overall damping ratio is the sum of the damping ratios due to Rayleigh damping and active vibration control. Since we are interested in studying the effect of various parameters on active damping, we henceforth neglect the Rayleigh damping effects. But it should be noted that in practice, if the structural damping were not present, instability would result in the system.

The term *axial* modes used in this paper comprises both longitudinal and transverse modes for a particular circumferential harmonic. No effort has been made to differentiate between the two. In practice, however, the transverse mode frequencies are much lower than the longitudinal mode frequencies. Hence, in the numerical studies, the transverse modes are the ones that are quoted.

### *5.1. Undamped Free Vibration Analysis*

Figure 2 shows the variation of in-plane normal strains (at $\theta = 0^o$ position) along the length of the shell. Shell I is considered here. From the figure, it is seen that the $S_{ss}$ strain is always maximum at the clamped end, whereas the $S_{\theta\theta}$ strain is always minimum at the clamped end. From equation (21), it is seen that (since $e_{31} = e_{32}$) the modal potential depends on the sum of $S_{ss}$ and $S_{\theta\theta}$. From Figure 2, it is seen that the sum of $S_{ss}$ and $S_{\theta\theta}$ is maximum at the clamped end only for the $n = 1$ modes. For higher axial mode numbers, this need not be the case. This trend is reflected in Figure 3.

Shell I is used for the analysis. Piezoelectric material is assumed to be pasted over the entire surface of the shell. Figure (3) shows the variation of modal potential (averaged over an element/patch) along the length of the shell for various axial ($n$) and circumferential ($m$) modes. The nondimensionalized distance ($s/L$) of the midpoint of the piezoelectric patch from the clamped end of the shell $L$ is the total length of the shell. The magnitude of the modal potential of the first axial mode corresponding to the first circumferential mode (Figure 3a)

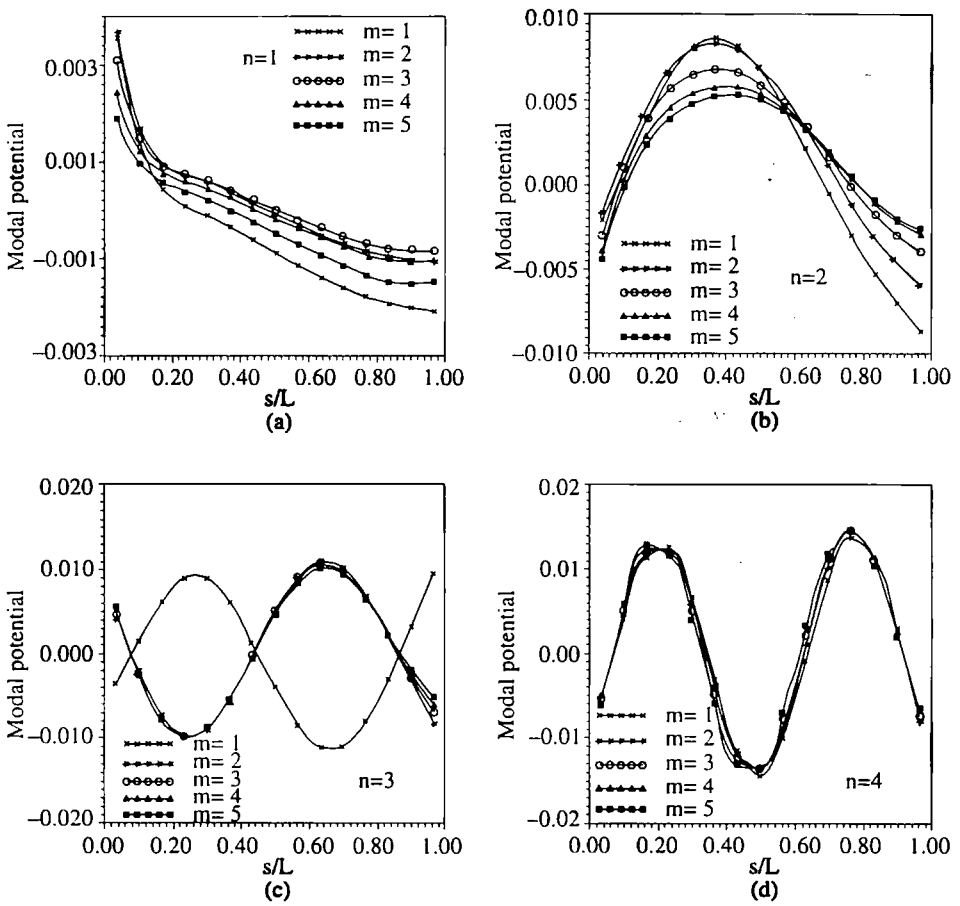


Figure 3. Variation of modal potential along the length of the shell for various circumferential and axial mode numbers.

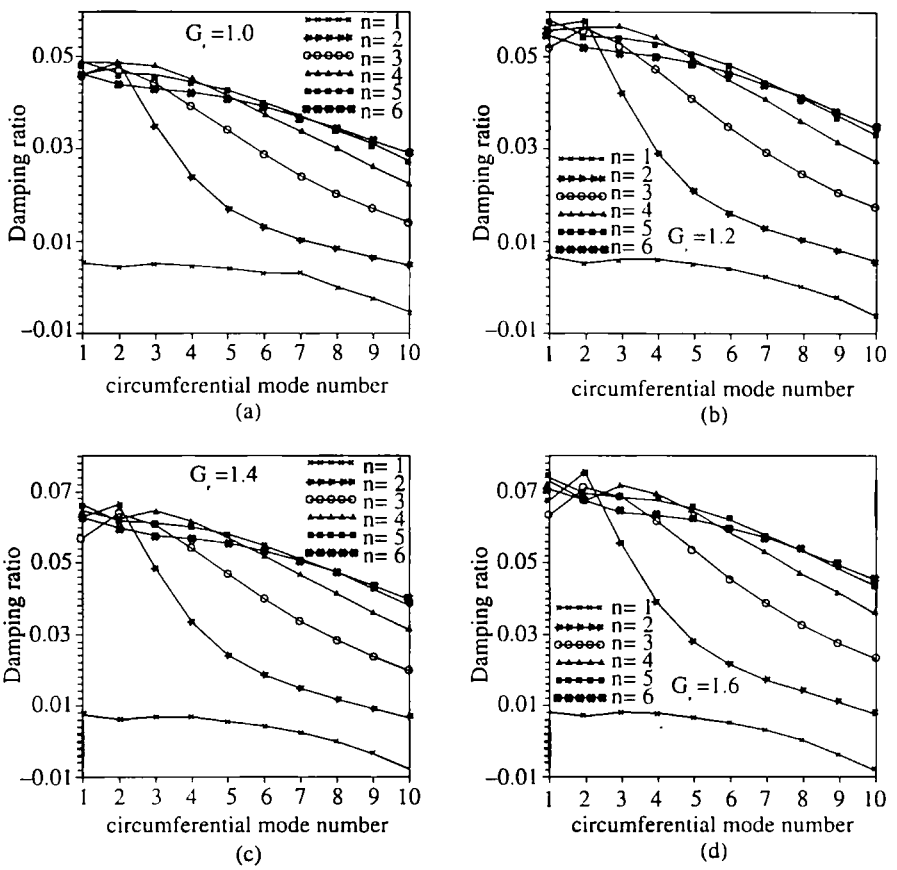


Figure 4. Variation of active damping ratio with circumferential mode number for various axial mode numbers and feedback factors, for Shell I (short shell).

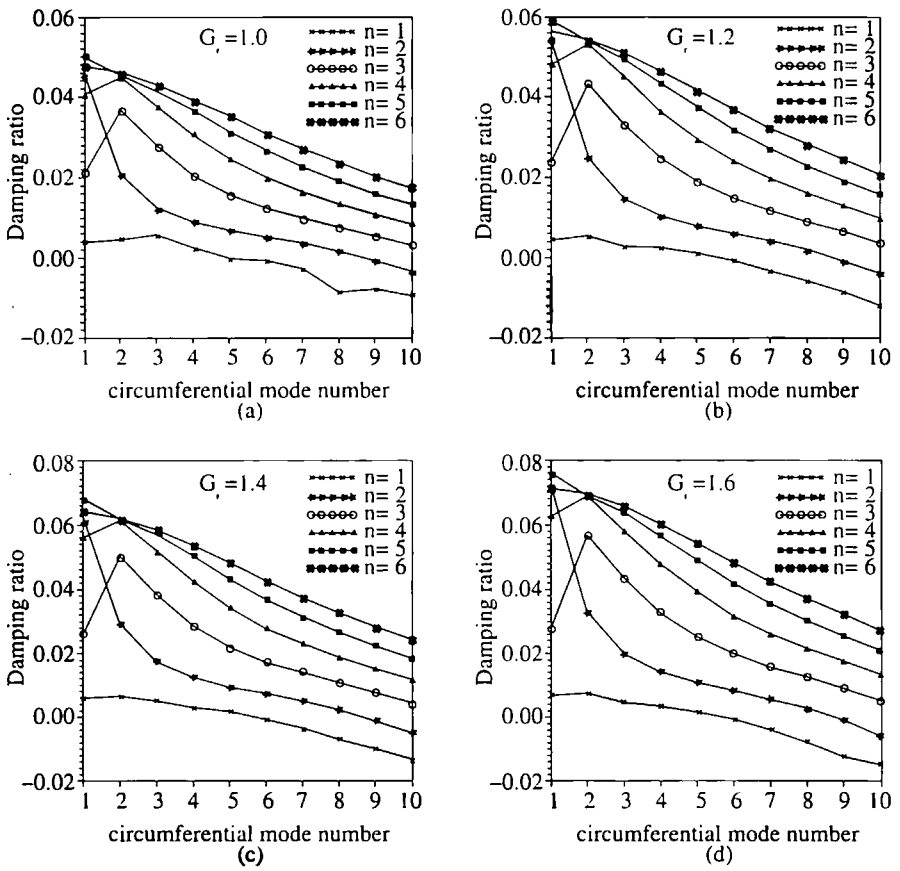


Figure 5. Variation of active damping ratio with circumferential mode number for various axial mode numbers and feedback factors, for Shell VII (tall shell).

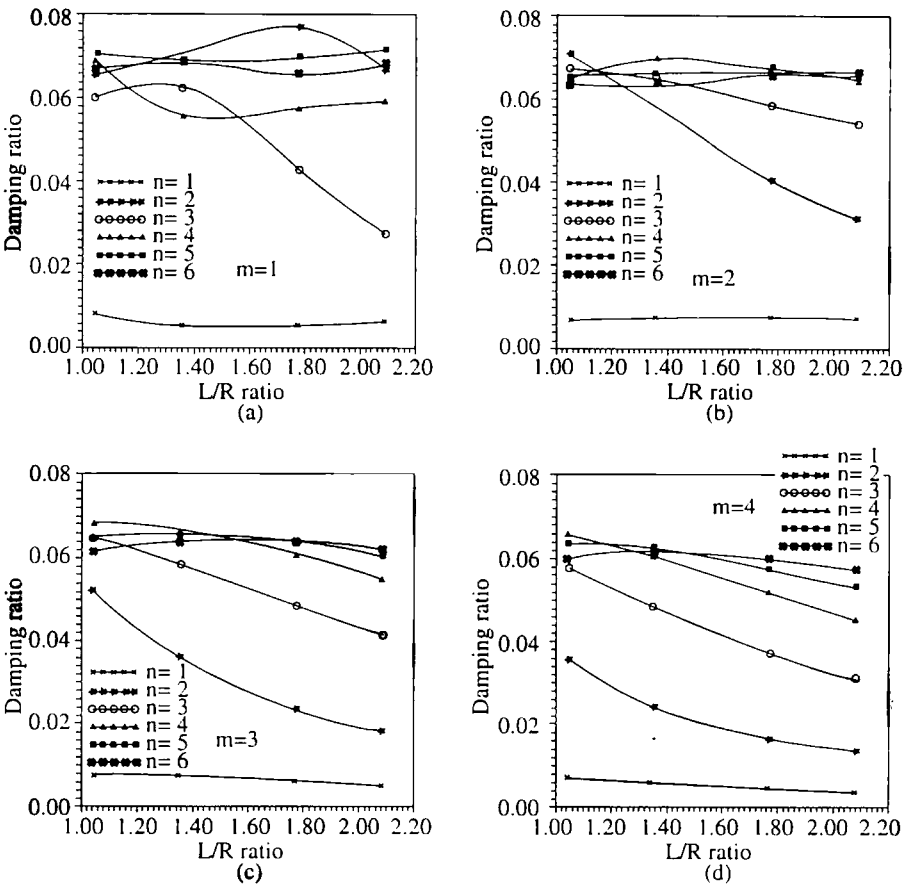


Figure 6. Variation of active damping ratio with length-to-radius ratio (L/R) of Shell I for various circumferential and axial mode numbers for a feedback factor of 1.5.

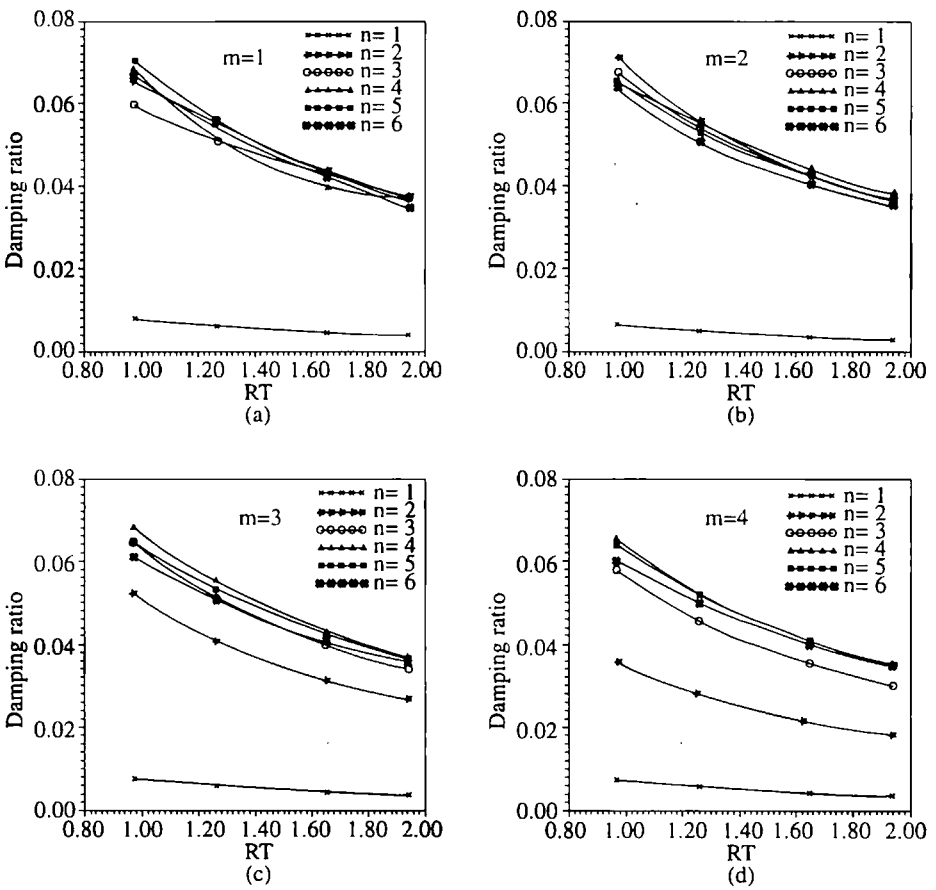


Figure 7. Variation of active damping ratio with radius-to-thickness ratio ($RT \times 10^2$) of Shell I for various circumferential and axial mode numbers for a feedback factor of 1.5.

is highest near the ends and zero in between. For higher circumferential modes, it is seen that the magnitude of the modal potential corresponding to the first axial mode is highest near the clamped end and least near the free end. For the second axial mode, the magnitude of the modal potential is maximum somewhere between the ends of the shell. The location of this peak varies with circumferential mode number. The number of peaks increases with increasing axial mode number. The rapidity of the variation is more for the higher axial mode numbers than the lower axial mode numbers. This rapid variation decreases with increase in circumferential mode number.

### *5.2. Variation of Active Damping Ratio ($\zeta$) With Circumferential ($m$) and Axial ($n$) Mode Numbers*

Figure 4 shows the variation of active damping ratio ($\zeta$) with circumferential and axial mode numbers for various feedback factors, for Shell I (short shell). From the figure, it is seen that $\zeta$ for the first axial mode does not vary much with circumferential mode number, up to the fifth circumferential mode number. Beyond that, it decreases steeply with increasing circumferential mode number. $\zeta$ corresponding to the second and third axial modes initially increases and then decreases with increasing circumferential mode number. $\zeta$ corresponding to the fourth axial mode (for circumferential mode $>$ 2) decreases, then increases and then decreases with increasing circumferential mode number. $\zeta$ for higher axial modes decreases steadily with circumferential mode number. For the lower circumferential modes, $\zeta$ corresponding to the first axial mode is very low when compared to that of higher axial modes. But this difference decreases for higher circumferential mode numbers. From Figure 4, it is seen that $\zeta$ corresponding to the first axial mode increases with increase in feedback factor ($G_F$) for lower circumferential modes, but decreases with increase in feedback factor for higher circumferential modes. $\zeta$ corresponding to higher axial modes increases with increase in $G_F$ for the range of $G_F$ considered. Figure 5 shows the variation of $\zeta$ with circumferential mode number for various axial mode numbers and feedback factors for Shell VII (tall shell). The difference in $\zeta$ between the first axial mode and higher axial modes for lower circumferential modes is not as prominent as for the short shell (Figure 4). For circumferential mode numbers less than 2, $\zeta$ increases with increasing axial mode number. $\zeta$ for the second axial mode decreases with increase in circumferential mode number. But for the short shell (Figure 4), $\zeta$ for the second axial mode initially increases and then decreases with increase in circumferential mode number. In general, for both tall and short shells, $\zeta$ decreases with increase in circumferential mode number beyond a certain circumferential mode number.

### *5.3. Effect of Length-to-Radius (L/R) Ratio and Radius-to-Thickness (R/T) Ratio of the Shell on the Active Damping Ratio*

Figure 6 shows the variation of $\zeta$ with L/R ratio for various circumferential ($m$) and axial ($n$) mode numbers, for a feedback factor of 1.5. Figure 6a corresponds to the first circumferential mode number. From this figure, it is seen that $\zeta$ corresponding to the first axial mode is very low and does not vary much with varying L/R ratio. $\zeta$ for the second and third axial modes initially increases and then decreases with increasing L/R ratio. $\zeta$ corresponding to the fifth

and sixth axial modes decreases gradually with increasing L/R ratio. $\zeta$ corresponding to the fourth axial mode decreases and then increases with increasing L/R ratio. Figure 6b corresponds to the second circumferential mode. $\zeta$ corresponding to the first axial mode is almost invariant with varying L/R ratio. $\zeta$ corresponding to the second and third modes decreases with increasing L/R ratio. $\zeta$ corresponding to higher axial modes varies gradually with L/R ratio. Figures 6c and 6f correspond to higher circumferential modes. The variation pattern of $\zeta$ with variation in L/R ratio for higher circumferential modes is similar to that for the second circumferential mode, except that the actual values of $\zeta$ decrease with increasing circumferential mode number. Also the variation of $\zeta$ with L/R ratio for the higher axial modes increases with increase in circumferential mode number.

Figure 7 shows the variation of $\zeta$ with R/t ratio of the shell, for various axial and circumferential mode numbers, for a feedback factor of 1.5. From the figure, it is seen that for lower circumferential mode numbers there is very little variation of $\zeta$ with varying axial mode number. But for higher circumferential mode numbers, there is a marked variation of $\zeta$ with varying axial mode number. In general, $\zeta$ decreases with increasing R/t ratio. This decrease is initially steep and then it is gradual. For the first axial mode, the decrease in $\zeta$ with R/t ratio is very gradual.

### *5.4. Effect of Percentage Area of the Shell Covered by Piezoelectric Material on the Active Damping Ratio ($\zeta$)*

In this study, the piezoelectric material is pasted throughout the circumference of the cylinder and partially along the axial direction. The percentage of the area that is covered by the piezoelectric material is varied by varying the regions along the length of the shell on which the piezoelectric layer is pasted. It is assumed that the piezoelectric material patch starts from the clamped end. Feedback constant is assumed to be 1.5. Figure 8 shows the variation of $\zeta$ with percentage area of the shell covered with piezoelectric material (sensors/actuators), for various circumferential and axial mode numbers. Figure 8a corresponds to the first circumferential mode number. From the figure, it is seen that $\zeta$ corresponding to the first axial mode increases very gradually with increase in percentage area covered. $\zeta$ for the second axial mode increases with increase in percentage area covered, up to 60%. From 60% to 80%, the increase in the area covered causes a decrease in $\zeta$. Beyond 80%, $\zeta$ increases with increase in percentage area covered. $\zeta$ for third and fifth axial modes initially increases gradually, then steeply, and again gradually with increase in percentage area covered. For the fourth axial mode, $\zeta$ initially increases, then decreases, and again increases with increase in percentage area covered. Figures 8c and 8f correspond to higher circumferential modes. From the figures, it is seen that the percentage area covered has very little effect on $\zeta$ for the first axial mode. For the second axial mode corresponding to $m > 2$, $\zeta$ increases with increase in percentage area covered, up to 60%. Beyond that, an increase in percentage area covered has little effect on $\zeta$. For higher axial modes, $\zeta$ increases with increasing percentage area covered.

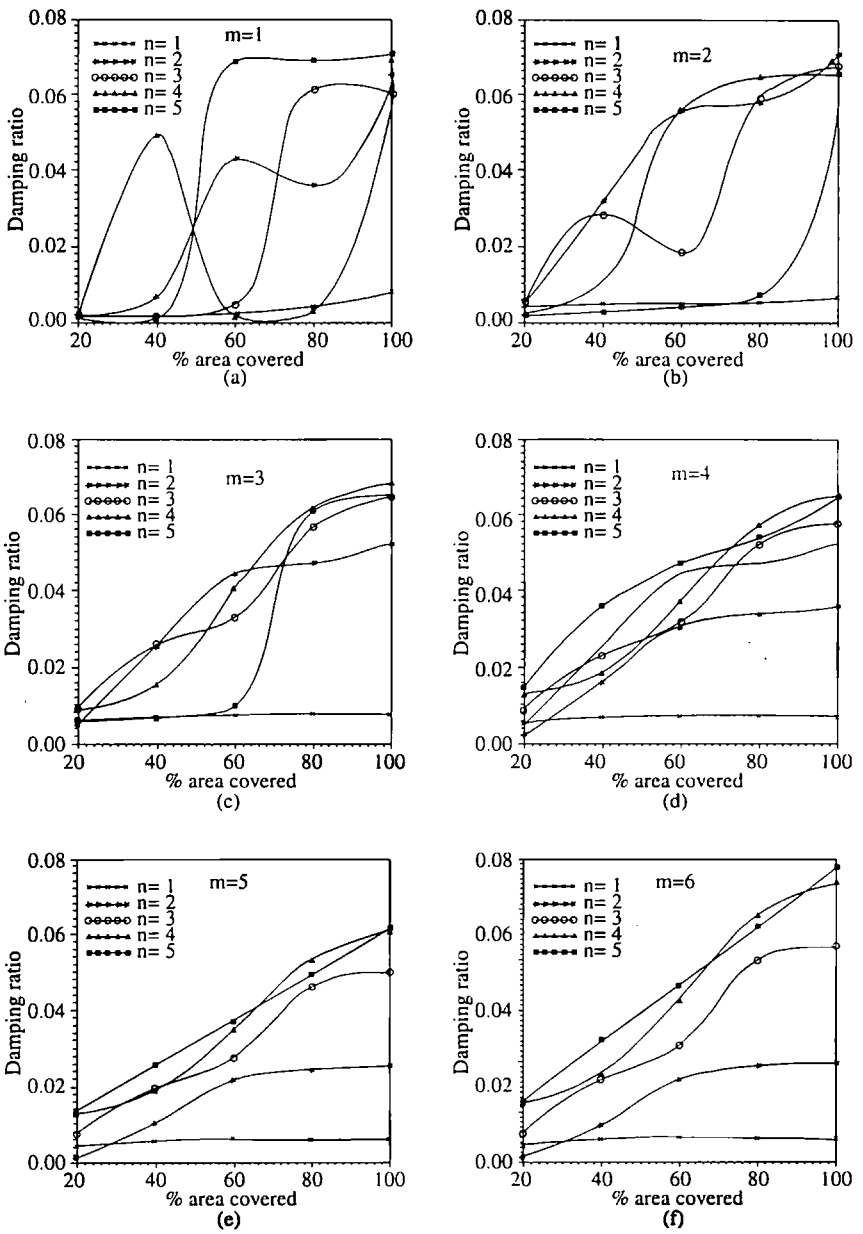


Figure 8. Variation of active damping ratio with percentage area of the shell (Shell I) covered with piezoelectric sensors/actuators for various circumferential and axial mode numbers for a feedback factor of 1.5.

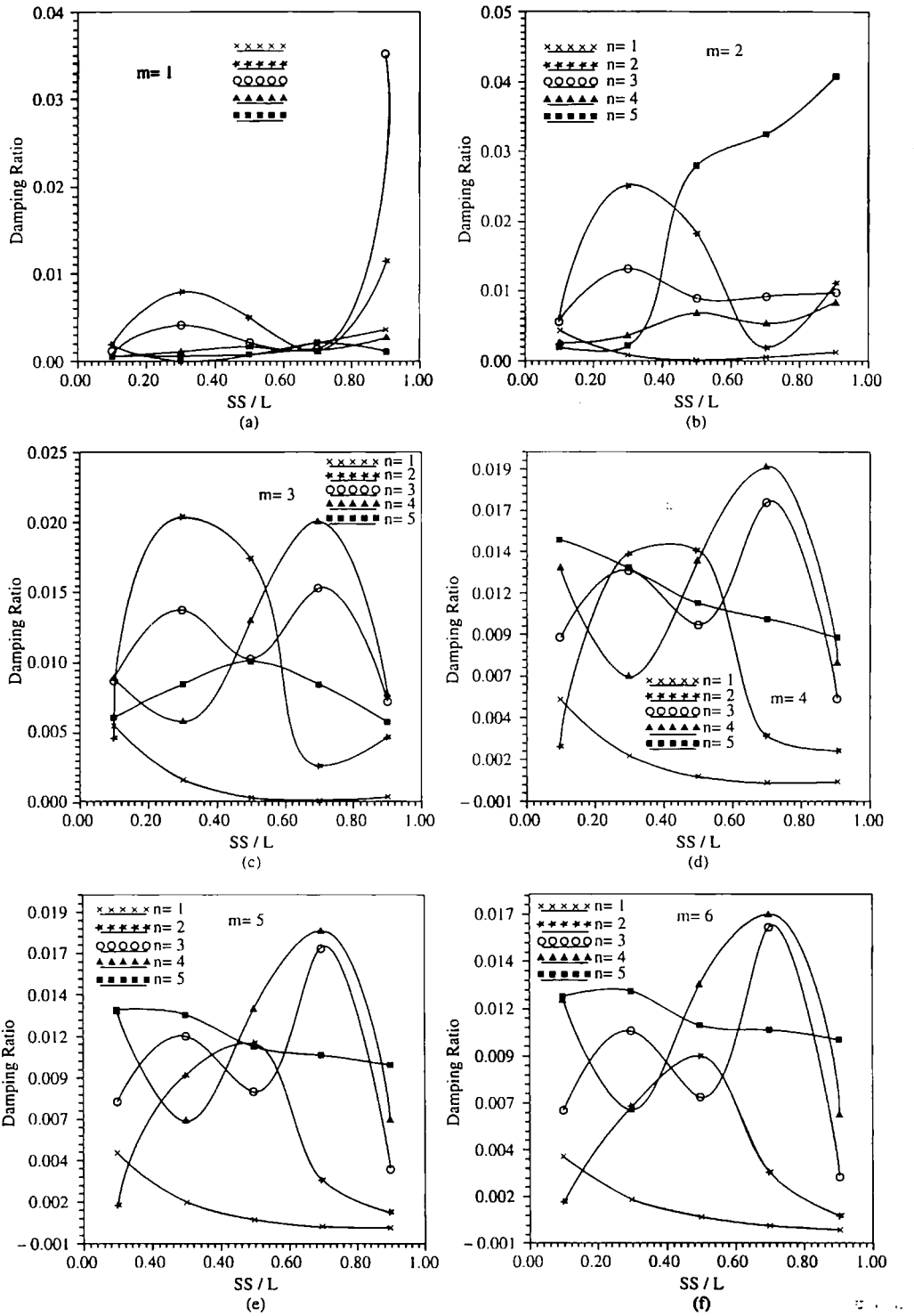


Figure 9. Variation of active damping ratio with location of the piezoelectric sensors/actuators on the shell (Shell I) for various circumferential and axial mode numbers for a feedback factor of 1.5.

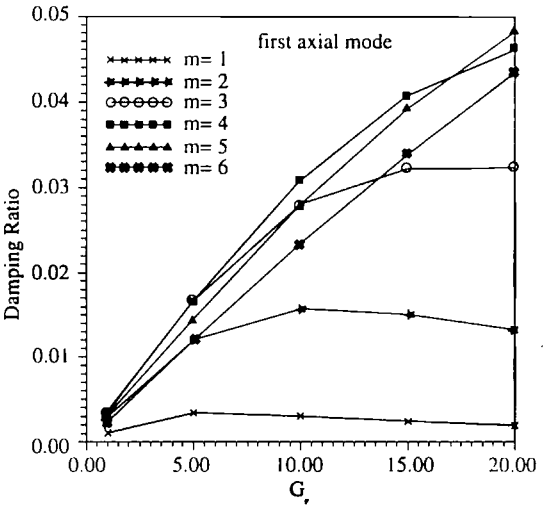


Figure 10. Variation of active damping ratio corresponding to first axial mode number with feedback factor for various circumferential mode numbers. (20% of the area of the shell from the clamped end is covered with piezoelectric layer.).

### *5.5. Effect of Location of Sensors/Actuators on the Active Damping Ratio*

Shell I is used for this study. In this study, only one-fifth of the length of the cylindrical shell is covered by piezoelectric material. But in the circumferential direction, the piezoelectric material is pasted all around. The distance of the midpoint of the piezoelectric patch length from the clamped end is denoted by ss. This is nondimensionalized with respect to the total length of the shell, L. The effect of the location of the patch along the cylinder length on $\zeta$ is studied. The patch consists of three collocated sensors and actuators along the length. The three collocated sensors and actuators are always placed subsequently, one after the other. Figure 9 shows the variation of $\zeta$ with ss/L for various axial and circumferential mode numbers, for a feedback factor of 1.5.

From Figure 9, it is seen that $\zeta$ corresponding to the first axial mode is generally high near the clamped end. The peak value of $\zeta$ for the second axial mode does not occur at the ends but at an intermediate point. For higher circumferential modes ($> 2$), $\zeta$ for $n = 3$ has two distinct peaks.

Figure 10 shows the variation of active damping ratio corresponding to first axial mode number with feedback factor for various circumferential mode numbers. In this case, the piezoelectric sensor/actuator patch is placed nearest the clamped end. From the figure, it is seen that for the range of feedback factors considered, $\zeta$ for the first and second circumferential modes increases and then decreases with increase in feedback factors. $\zeta$ corresponding to higher circumferential modes increases with increase in feedback factor. Except for the first and second circumferential modes, it is possible to obtain a value of $\zeta$, greater than 2%, for the other circumferential modes.

## 6. CONCLUSIONS

The effect of various parameters on the active damping ratio of the smart cylindrical shell has been studied. The study has resulted in the following general conclusions:

1 Active damping ($\zeta$) ratio decreases with increasing circumferential mode number, for higher circumferential mode numbers.
2 Covering the entire surface of the shell with piezoelectric material (sensors/actuators) has very little effect on $\zeta$ corresponding to the first axial mode.
3 In the case of the short shell for the lower circumferential modes, there is very little difference between the damping ratios corresponding to higher axial modes. But for the tall shell, this difference is marked.
4 $\zeta$ decreases with increasing radius-to-thickness ratio of the cylindrical shell.
5 For some of the modes, it is seen that the percentage area of the shell covered by piezoelectric material has no effect on $\zeta$, beyond a certain percentage.
6 The magnitude of the active damping ratio is affected by the location of the collocated piezoelectric sensor/actuator patches. An attempt could be made to draw a correlation between the variation in modal potential along the length of the shell and the variation of $\zeta$ with location of the sensors/actuators.

## REFERENCES

Allik, H. and Hughes, T.J.R., 1970, "Finite element method for piezoelectric vibration," *International Journal for Numerical Methods in Engineering* **2**, 151-157.

Baruch, P. and Abramovich, H., 1997, "Consistent methodology for the modelling of piezolaminated shells," *AIAA Journal* **35**(8), 1316-1326.

Callahan, J. and Baruh, H., 1996, "Vibration monitoring of cylindrical shells using piezoelectric sensors," *Finite Elements in Analysis and Design* **23**, 303-318.

Heyliger, P., Pei, K. C., and Saravanos, D., 1996, "Layerwise mechanics and finite element model for laminated piezoelectric shells," *AIAA Journal* **34**(11), 2353-2360.

Hussein, M. and Heyliger, P. R., 1996, "Discrete layer analysis of axisymmetric vibrations of laminated piezoelectric cylinders," *Journal of Sound and Vibration* **192**(3), 995-1013.

Lee, C. K. and Moon, F. C., 1990, "Modal sensors/actuators," *ASME Journal of Applied Mechanics* **57**, 434-441.

Saravanos, D., 1997, "Mixed laminate theory and finite element for smart piezoelectric composite shell structures," *AIAA Journal* **35**(8), 1327-1333.

Sonti, V. and Jones, J. D., 1996, "Curved piezoactuator model for active vibration control of cylindrical shells," *AIAA Journal* **34**(5), 1034-1040.

Sung, C. K., Chen, T. F., and Chen, S. G., 1996, "Piezoelectric modal sensor/actuator design for monitoring/generating flexural and torsional vibrations of cylindrical shells," *ASME Journal of Vibration and Acoustics* **118**, 48-55.

Tzou, H. S., 1991, "Distributed modal identification and vibration control of continua: Theory and applications," *ASME Journal of Dynamic Systems, Measurement and Control* **113**, 494-499.

Tzou, H. S., Bao, Y., and Venkayya, V. B., 1996, "Parametric study of segmented transducers laminated on cylindrical shells, Part 2: Actuator patches," *Journal of Sound and Vibration* **197**(2), 225-249.

Tzou, H. S. and Howard, R. V., 1994, "A piezothermoelastic thin shell theory applied to active structures," *ASME Journal of Vibration and Acoustics* **116**, 295-302.

Tzou, H. S. and Tseng, C. I., 1990, "Distributed piezoelectric sensor/actuator design for dynamic measurement/control of distributed parametric systems: A piezoelectric finite element approach," *Journal of Sound and Vibration* **138**(1), 17-34.

Tzou, H. S. and Ye, R., 1996, "Analysis of piezoelectric structures with piezoelectric triangle shell elements," *AIAA Journal* **34**(1), 110-115.

Tzou, H. S., Zhong, J. P., and Natori, M., 1993, "Sensor mechanics of distributed shell convolving sensors applied to flexible rings," *ASME Journal of Vibration and Acoustics* **115**, 40-46.

Xu, K. and Noor, A. K., 1996, "Three-dimensional analytical solutions for coupled thermoelectroelastic response of multilayered cylindrical shell," *AIAA Journal* **34**(4), 802-812.

Zheng, Z. C., Ren, G. X., and Wang, W. J., 1997, "A Reduction method for large scale unsymmetric eigenvalue problems in structural dynamics," *Journal of Sound and Vibration* **199**(2), 253-268.